

# Biofunctional polymer nanoparticles for intra-articular targeting and retention in cartilage

DOMINIQUE A. ROTHENFLUH<sup>1</sup>, HARRY BERMUDEZ<sup>1,2</sup>, CONLIN P. O'NEIL<sup>1</sup> AND JEFFREY A. HUBBELL<sup>1\*</sup>

<sup>1</sup>Institute of Bioengineering and Institute of Chemical Sciences and Engineering, Ecole Polytechnique Fédérale de Lausanne, CH-1015 Lausanne, Switzerland

<sup>2</sup>Department of Polymer Science and Engineering, University of Massachusetts, Amherst, Massachusetts 01003, USA

\*e-mail: jeffrey.hubbell@epfl.ch

Published online: 3 February 2008; corrected online 12 February 2008; doi:10.1038/nmat2116

The extracellular matrix of dense, avascular tissues presents a barrier to entry for polymer-based therapeutics, such as drugs encapsulated within polymeric particles. Here, we present an approach by which polymer nanoparticles, sufficiently small to enter the matrix of the targeted tissue, here articular cartilage, are further modified with a biomolecular ligand for matrix binding. This combination of ultrasmall size and biomolecular binding converts the matrix from a barrier into a reservoir, resisting rapid release of the nanoparticles and clearance from the tissue site. Phage display of a peptide library was used to discover appropriate targeting ligands by biopanning on denuded cartilage. The ligand WYRGL was selected in 94 of 96 clones sequenced after five rounds of biopanning and was demonstrated to bind to collagen II  $\alpha 1$ . Peptide-functionalized nanoparticles targeted articular cartilage up to 72-fold more than nanoparticles displaying a scrambled peptide sequence following intra-articular injection in the mouse.

Polymeric nanoparticles have been designed to augment drug concentrations in blood or vascularized tissues and aim to reduce a drug's toxicity and to improve its therapeutic effects<sup>1–4</sup>. Our interest here is delivery and targeting of nanoparticles to a distinctly avascular tissue, namely articular cartilage. The lack of vascularity points towards regional administration within the joint space, rather than administration into the systemic circulation. Clearance of drug from the synovial fluid into the draining lymphatics is efficient, however, limiting residence times to as short as 1–5 h (ref. 5). We focus our attention on particles that are sufficiently small to enter the cartilage matrix, as it is dynamically compressed during normal ambulation, and that display biomolecular affinity for a cartilage extracellular matrix (ECM) component so as to be retained there. The particles must indeed be small, given the about 60 nm mesh size of the collagen II fibrillar network<sup>6</sup> and the about 20 nm spacing between the side chains of the proteoglycan network<sup>7</sup> of cartilage. With such nanoparticle penetration and retention, the structure of cartilage would be turned from a barrier into a reservoir.

We have used the powerful technique of phage display<sup>8–11</sup> and carried out affinity selection, so-called biopanning<sup>12</sup>, on sliced bovine cartilage to develop such a biomolecular targeting feature for nanoparticle functionalization. We sought to functionalize nanoparticles that are capable of carrying a hydrophobic drug payload, such as a small-molecule inhibitor of aggrecanases involved in cartilage degradation in osteoarthritis<sup>13–17</sup>. We chose to work with nanoparticles of poly(propylene sulphide) (PPS), developed in our laboratory<sup>18</sup>, because their synthesis by inverse emulsion polymerization lends itself to surface functionalization and because size control ranging from 20 to 200 nm can be achieved simply by adjusting the emulsifier-to-monomer ratio. Peptides discovered to have affinity can thus be

covalently grafted to the emulsifier, namely the block copolymer poly(ethylene glycol)-*bl*-poly(propylene glycol)-*bl*-poly(ethylene glycol) (commonly referred to as Pluronic) which will remain on the surface after inverse emulsion polymerization<sup>19</sup>.

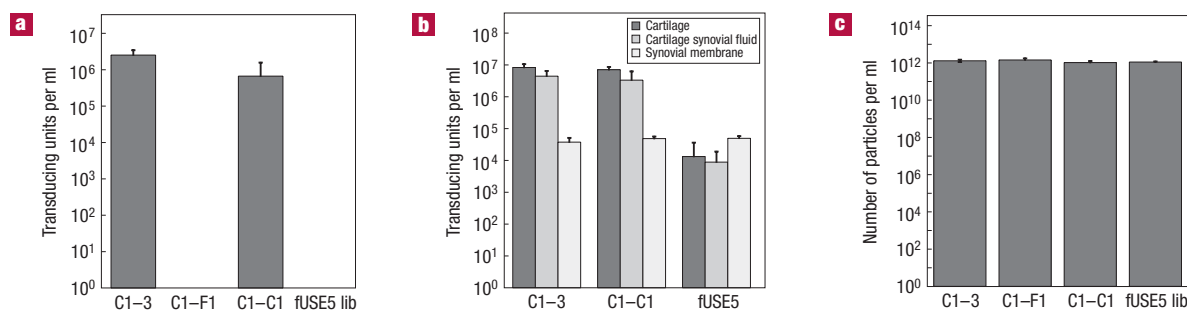
Here, we report the development of a novel nanoparticle-based drug-delivery system for intra-tissue drug release in articular cartilage through the discovery of a ligand specific for articular cartilage that was found to target the cartilage matrix component collagen II  $\alpha 1$ . Immobilization of this ligand on 38-nm-diameter PPS nanoparticles led to up to a 72-fold increase in targeting the extracellular compartment of articular cartilage in the mouse. This approach provides a route to target an otherwise poorly accessible avascular tissue and may prove useful in drug and biomolecular therapy in diseases such as osteoarthritis<sup>20</sup>.

## RESULTS

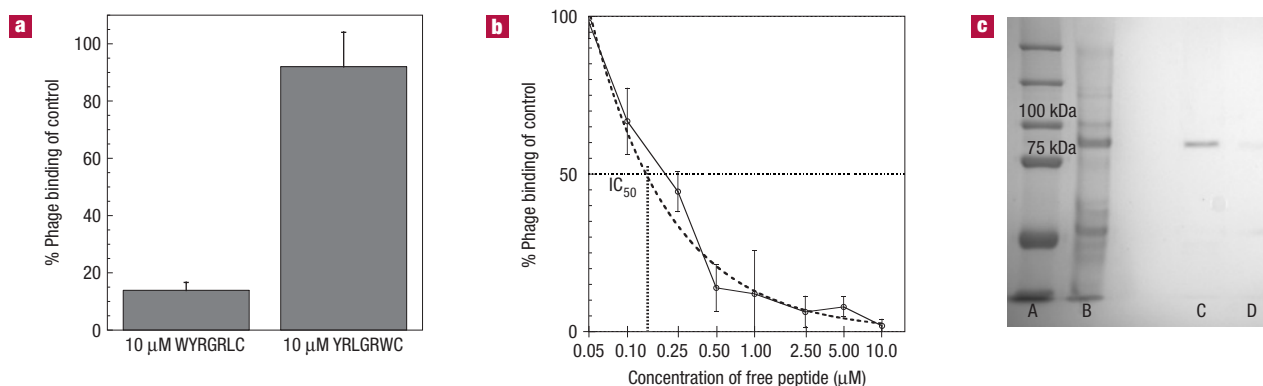
### BIOPANNING OF PHAGE DISPLAY LIBRARY FOR CARTILAGE AFFINITY AND BINDING ASSAYS

Affinity selection (biopanning) was carried out on denuded bovine cartilage grafts, which were incubated with the fUSE5 peptide-on-phage display library<sup>21</sup> expressing linear 6-mer random peptides on minor coat proteins (pIII) of fd-phage with a diversity of  $6.4 \times 10^7$  (G. P. Smith Lab, University of Missouri, Columbia, USA). After round 3, sequencing of 32 clones did not reveal a consensus motif in the selected peptides. Sequencing of 96 clones after round 5 yielded three different phage clones, C1–3, C1–C1 and C1–F1, displaying the peptides Trp-Tyr-Arg-Gly-Arg-Leu, Asp-Pro-His-Phe-His-Leu and Arg-Val-Met-Leu-Val-Arg, respectively. C1–3 appeared in 94 sequenced clones, and both C1–C1 and C1–F1 appeared only once (sequences given in Supplementary Information, Table S1).

A competitive binding assay was carried out to assess the relative binding strengths of the selected phage clones against each other.



**Figure 1** Phage amplification and competitive binding showing that C1–3 was selected owing to its specificity of binding to the cartilage matrix. **a**, The competitive binding assay in which only phage clones C1–3 and C1–C1 could be recovered. **b**, Binding specificity of C1–3 and C1–C1 to articular cartilage. Binding of these phage clones to synovial membrane results in a lower phage recovery by two orders of magnitude, reflecting non-specific binding, which is demonstrated by the random library as a control. On the basis of the negative screens in round 1, adding synovial fluid does not impair binding of C1–3 to its target. **c**, Overnight amplification of the three phage clones ( $10^6$  particles  $\text{ml}^{-1}$ ) identified in the fifth round of biopanning showing that they all grow at equal rates comparable to the random library. Final selection of C1–3 was therefore not affected by differences in growth during amplification. Bars indicate mean  $\pm$  s.d. from three independent experiments.



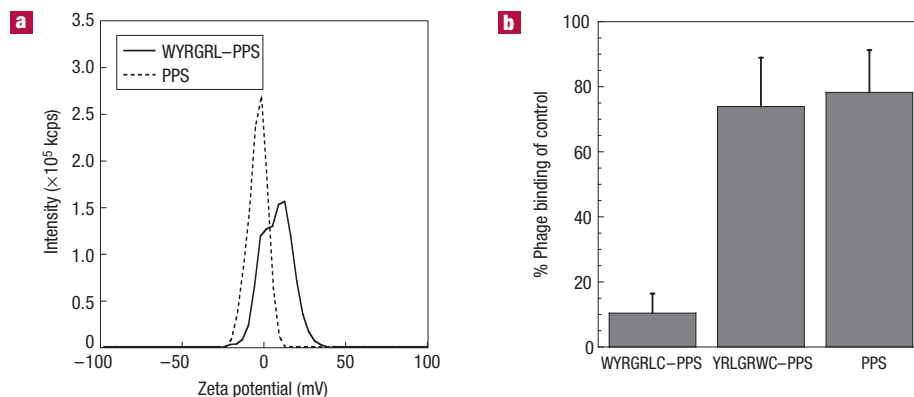
**Figure 2** Competitive and sequence-specific binding of WYRGRL. **a**, Inhibition of cartilage binding of WYRGRL-displaying phage (C1–3) by the synthetic peptides WYRGRLC and YRLGRWC. A concentration of  $10 \mu\text{M}$  of WYRGRLC resulted in a decrease of phage binding to  $13.9 \pm 2.8\%$ , whereas YRLGRWC did not cause a significant drop of phage titre ( $92.0 \pm 12\%$ ) (mean  $\pm$  s.d.). **b**, Competitive binding of C1–3 against serial dilutions of WYRGRLC resulted in a dose-response curve. An  $\text{IC}_{50}$  of  $140 \text{ nM}$  was calculated from the fitted curve (dashed line). Data represent the percentage of maximal phage binding of clone C1–3 obtained in the absence of synthetic peptide. Bars indicate mean  $\pm$  s.d. from three independent experiments. Curve fit  $y = 12.878 \times x^{-0.69099}$   $R = 0.98807$ . **c**, SDS-PAGE of digested cartilage matrix (lane B) and eluates after affinity purification on WYRGRL (lane C) and YRLGRW (lane D) columns. Lane A is a molecular-weight marker. Lane C shows a single strong band, whereas lane D retained little of the corresponding protein as indicated by the faint band. WYRGRL therefore binds to one specific target, which is identified as collagen II  $\alpha 1$  by infusion ion-trap mass spectrometry and binding is sequence specific.

Figure 1a shows that only C1–3 and C1–C1 have been recovered owing to their superior binding strength. In addition, C1–3 had an almost one order of magnitude higher titre count than C1–C1, which further demonstrates its dominant binding as was already indicated by its frequent appearance after round 5 of biopanning.

The binding specificity of C1–3 and C1–C1 to articular cartilage was evaluated by exposing the phage clones to articular cartilage and an equivalent surface area of synovial membrane. Figure 1b shows that both C1–3 and C1–C1 exhibit specific binding to articular cartilage over synovial membrane by two orders of magnitude and that the addition of synovial fluid does not yield a significant drop in phage binding to articular cartilage. No background phage binding to polystyrene was detectable. That the observed differences in phage numbers were not artefactually due to differences in phage multiplication rate is demonstrated in Fig. 1c, where no significant differences in growth were observed. Affinity

selection of the fUSE5/6-mer phage display library resulted in the discovery of three phage clones, of which C1–3 (peptide WYRGRL) exhibits both dominant binding compared with other phage clones and binding specificity to articular cartilage (Fig. 1a,b). Therefore, the peptide WYRGRL and its scrambled sequence YRLGRW were synthesized with a cysteine at the carboxy (C) terminus (that is, WYRGRLC and YRLGRWC), which is used for bioconjugation to vinyl-sulphone-derivatized polymers via the free thiol through Michael-type addition<sup>22</sup>.

A competitive binding assay of the phage clone C1–3 against the corresponding free peptide and its scrambled sequence was carried out. At a concentration of  $10 \mu\text{M}$ , WYRGRLC resulted in a decrease of C1–3 phage titre to  $13.9 \pm 2.8\%$  (Fig. 2a). On the other hand,  $10 \mu\text{M}$  of the scrambled sequence YRLGRWC did not decrease the phage titre ( $92.0 \pm 12\%$ ). These results indicate that the interaction between the sequence WYRGRL and its ligand is sequence specific



**Figure 3** Characterization of peptide-conjugated nanoparticles. Peptides with a cysteine at the C terminus were conjugated by Michael-type addition to Pluronic–di-vinyl sulphone, which was used as the emulsifier in nanoparticle synthesis and remains on the particle surface after synthesis and purification. **a**, The presence of the positively charged peptide WYRGRL on the nanoparticle surface was confirmed by measurement of the zeta potential. Non-conjugated particles showed a zeta potential around neutral ( $-2.64 \pm 8.97$  mV, dashed line), whereas conjugated nanoparticles shifted the zeta potential to a positive value ( $+17.8 \pm 3.45$  mV, solid line). **b**, Competitive binding of nanoparticles against phage C1–3. WYRGRL–PPS nanoparticles decreased phage binding to  $10.4 \pm 6\%$ , whereas YRLGRW–PPS and PPS nanoparticles did not show a marked decrease in phage binding to cartilage. Bars indicate mean  $\pm$  s.d. from three independent experiments.

rather than mediated by charge alone, for example. A dose-response curve was determined by serial dilution of the peptide ranging from 50 nM to 10  $\mu$ M and mixing them with  $10^8$  transducing units per millilitre of phage. The titre counts of phage recovered gradually decreased by increasing the concentration of the free peptide in solution. A half-maximal inhibitory concentration ( $IC_{50}$ ) of 140 nM is calculated from the curve in Fig. 2b.

#### AFFINITY PURIFICATION AND PROTEIN IDENTIFICATION

Affinity chromatography against the peptide WYRGRL was carried out to identify its potential ligand in the cartilage matrix (see the Supplementary Information). Stepwise elution to 500 mM KCl resulted in a single band in the eluate of the WYRGRL column, as shown by SDS–polyacrylamide gel electrophoresis (SDS–PAGE; Fig. 2c, lane C). The same band was only faintly present in the eluate for the mismatch sequence (Fig. 2c, lane D), further supporting the idea of a sequence-specific, non-covalent interaction. The bands correspond to a strong band in the cartilage matrix (Fig. 2c, lane B) and therefore are likely to represent an abundant ECM protein. Analysis of the in-gel digested band by mass spectrometry revealed collagen II  $\alpha 1$  (bovine, P02459) in two samples from different purifications (see Supplementary Information, Table S1 and Fig. S1). Collagen II  $\alpha 1$  is therefore identified as the binding partner of WYRGRL, which as a consequence provides a means to target and immobilize polymeric nanoparticles in the collagen II network of articular cartilage.

#### CONJUGATION OF PEPTIDE TO PLURONIC F-127 AND NANOPARTICLE SYNTHESIS

Functionalized nanoparticles were synthesized with 10% peptide-conjugated Pluronic F-127 (see Supplementary Information, Fig. S2 for size distributions), which caused a shift in the zeta potential from about neutral ( $-2.64 \pm 8.97$  mV) for non-conjugated PPS nanoparticles to  $+17.8 \pm 3.45$  mV, which confirms the presence of the peptide on the nanoparticle surface (Fig. 3a).

To determine whether the sequence WYRGRLC would retain its targeting and binding capacity when conjugated to the nanoparticle surface, WYRGRL–PPS and YRLGRW–PPS nanoparticles at 2% (w/v) were subjected to a competitive binding assay against phage C1–3. The results shown in Fig. 3b demonstrate that WYRGRL–PPS nanoparticles decrease phage binding to  $10.4 \pm 6\%$  and

therefore exhibit similar binding as the corresponding free peptide WYRGRLC ( $13.9 \pm 2.8\%$ , Fig. 2a). YRLGRW–PPS nanoparticles did not bind competitively and thus did not result in a comparable drop of phage titre ( $73.9 \pm 15\%$ ), which corresponds to the non-specific decrease of non-conjugated PPS nanoparticles ( $78.3 \pm 13\%$ ). WYRGRL–PPS nanoparticles at a degree of surface functionalization of 10% at 2% (w/v) therefore seem to have similar binding affinity to articular cartilage as the free peptide WYRGRLC at 10  $\mu$ M when compared with phage binding.

#### ACTIVE TARGETING OF ARTICULAR CARTILAGE *IN VIVO*

Nanoparticle formulations were injected intra-articularly into the knees of mice, and confocal laser scanning microscopy was used to quantify nanoparticle localization and retention. To normalize fluorescence levels, the settings of the confocal microscope were adjusted on labelled nanoparticles (see Supplementary Information, Fig. S3). Particles that entered the cartilage were observed both in the matrix compartment and within chondrocytes (Fig. 4). The pericellular matrix and the cell nuclei were substantially free of nanoparticles. Although both targeted and non-targeted nanoparticles, that is, WYRGRL–PPS (green) and YRLGRW–PPS (red), respectively, could be found in cells at similar levels, targeted nanoparticles were immobilized in the matrix to a much greater extent, which can be seen well in the merged images (Fig. 4c,f,i). Quantification of background-subtracted integrated fluorescence per cartilage volume was carried out separately for the intracellular and extracellular compartments and was determined by sampling  $z$  stacks with 10 planes ( $z$  dimension 6.94  $\mu$ m) in 10 different locations per joint. Quantification of nanoparticle accumulation by integrated fluorescence in the extracellular space revealed dramatically more targeted nanoparticles than non-targeted. There was a 44.8-fold higher ( $t$ -test, one-tailed, paired,  $p = 0.011$ ,  $n = 3$ ; deviation from normality not significant by Shapiro Wilk's test, red  $p = 0.136$ , green  $p = 0.451$ ) targeted nanoparticle accumulation after 24 h, and a 71.7-fold mean increase ( $t$ -test, one-tailed, paired,  $p = 0.006$ ,  $n = 3$ ) after 48 h (Fig. 5a,c), comparing targeted with non-targeted nanoparticles. After 96 h, there was a mean 27.6-fold more integrated fluorescence for the green targeted nanoparticles in the ECM than for red non-targeted nanoparticles ( $t$ -test, one-tailed,

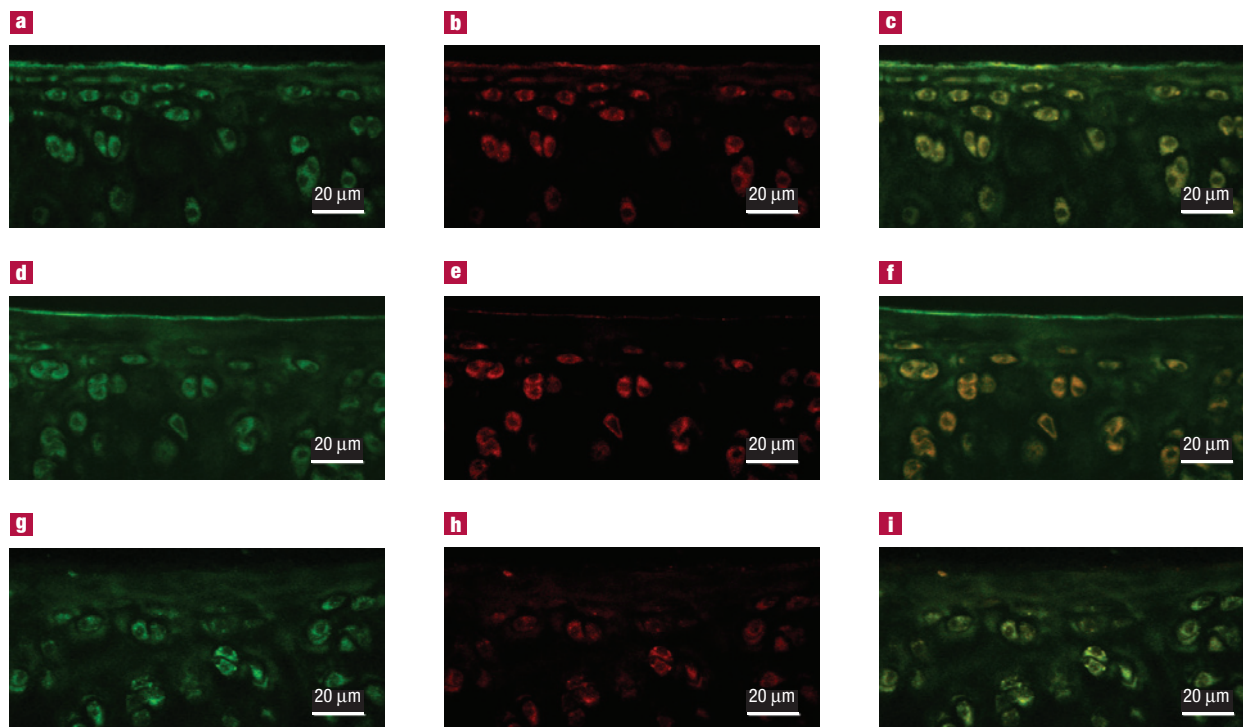


**Figure 4** *In vivo* targeting of WYRGRL-PPS nanoparticles. **a–i**, Nanoparticle distribution in articular cartilage after 24 h (**a–c**), 48 h (**d–f**) and 96 h (**g–i**). The green channel (**a,d,g**) represents WYRGRL-PPS labelled with 6-fluorescein-iodoacetamide, and the red channel (**b,e,h**) its mismatch, YRLGRW-PPS nanoparticles labelled with 5-tetramethylrhodamine-iodoacetamide, both of which were injected together into the same joint. Images **c,f,i** represent merged images of red and green channels. WYRGRL-PPS and YRLGRW-PPS enter the cartilage matrix as well as chondrocytes. Note that the pericellular matrix rich in collagen VI does not immobilize the nanoparticles and therefore is substantially spared of nanoparticles as well as the nuclei into which the particles do not seem to penetrate efficiently (best seen in images **c,f,i**). All images presented for illustration are non-background-subtracted summation images.

paired,  $p = 0.274$ ,  $n = 3$ ), which was not significant at  $p < 0.05$  owing to high variance in the measurements. Within the cells, there was a mean 3.7-fold higher accumulation of targeted nanoparticles than non-targeted after 24 h ( $t$ -test, one-tailed, paired,  $p = 0.003$ ,  $n = 3$ ), 5.0-fold more after 48 h ( $t$ -test, one-tailed, paired,  $p = 0.050$ ,  $n = 3$ ) and 4.2-fold more after 96 h ( $t$ -test, one-tailed, paired,  $p = 0.017$ ) (Fig. 5b,c). Interestingly, the ratio of extracellular versus intracellular accumulation ranged from 1.9 to 3.3 for the targeted and from 0.23 to 0.38 for the non-targeted nanoparticles (Fig. 5d), indicating that there are more targeted nanoparticles in the cartilage ECM than in the cells as opposed to more non-targeted nanoparticles in the cells than in the ECM, thus confirming the visual observation mentioned above. In addition, the possibility that observed differences in nanoparticle accumulation appear as an artefact of fluorescence emission rather than specific nanoparticle binding can be ruled out on the basis of the ratios in Fig. 5c, as the same ratios would be expected in both the extracellular and intracellular compartments if such an effect were present. The level of integrated fluorescence for the red non-targeted nanoparticles remained constant throughout the observation period of 96 h, for both the extracellular (analysis of variance (ANOVA), one-tailed,  $p = 0.591$ ,  $n = 3$ ; homogeneity of variance criteria met by Levene's test) and intracellular (ANOVA, one-tailed,  $p = 0.244$ ,  $n = 3$ ) compartments. Analysis of variance of the levels of integrated fluorescence for the green targeted nanoparticles suggests significant differences throughout the observation period for both the extracellular (ANOVA, one-tailed,  $p = 0.028$ ,  $n = 3$ ) and intracellular (ANOVA,

one-tailed,  $p = 0.039$ ,  $n = 3$ ) compartments. However, a post-hoc test to account for multiple testing using the Bonferroni method did not reveal significances between the time points, reflecting experimental variances rather than a true clearance of the nanoparticles throughout the observation period; in other words, statistically, the accumulation of targeted nanoparticles in the extracellular compartment was stationary over the 96 h period of observation.

In addition to functionalization versus non-functionalization at constant size, we also compared nanoparticles of 38 nm average size with particles of 96 nm average size, both displaying WYRGRL on their surface and labelled with 6-fluorescein-iodoacetamide and 5-tetramethylrhodamine-iodoacetamide, respectively. As is shown in Fig. 6a, nanoparticles around 96 nm in size are withheld in the superficial dense collagen II network of the cartilage surface after 24 h. Compared with the smaller nanoparticles, they seem unable to enter the cartilage matrix, which is reflected in a 14.9-fold higher mean integrated fluorescence for the particles 38 nm in size (Fig. 6b,  $t$ -test, one-tailed, paired,  $p = 0.037$ ,  $n = 4$ ). Overall, the *in vivo* results show that targeting articular cartilage via the collagen II network results in a higher particle accumulation and retention in the cartilage matrix and that this effect is dependent on the particle size being sufficiently small to pass through the dense ECM.

## DISCUSSION

The bioavailability of drugs in the cartilage matrix is limited by the avascularity of the tissue, and the dense ECM, which acts as

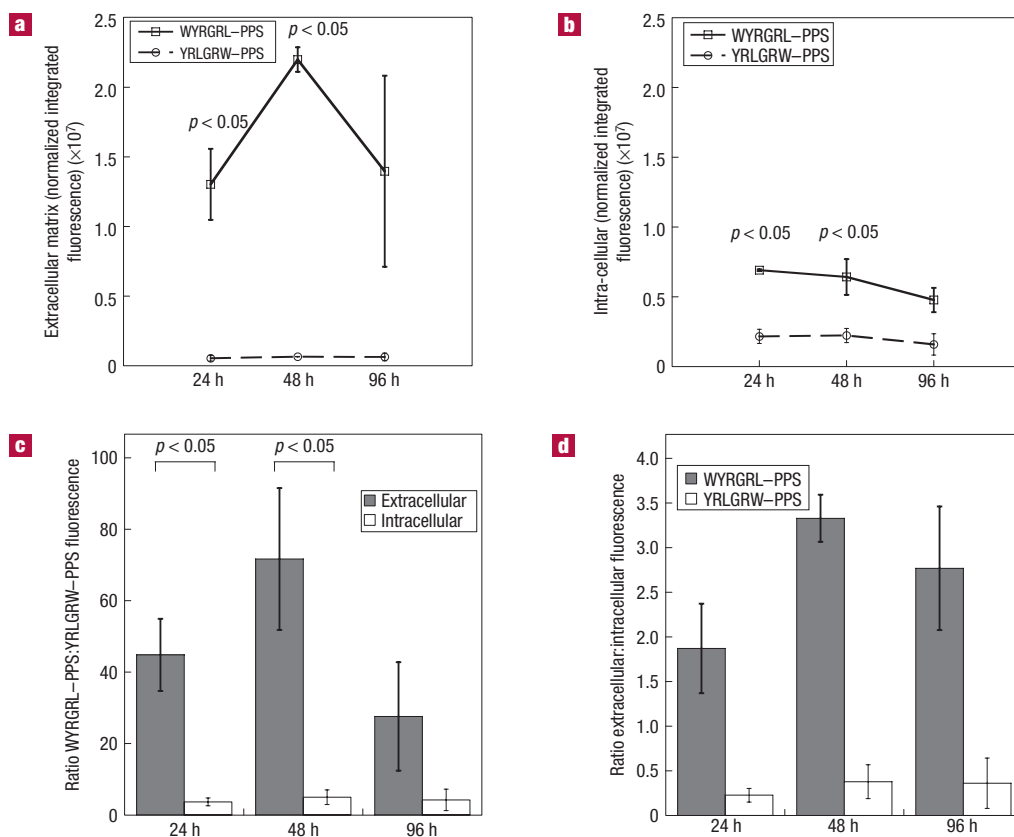


**Figure 5** Quantification of nanoparticles in the ECM and within the cells. **a**, Normalized mean integrated fluorescence in the ECM is significantly higher for targeted WYRGRL-PPS after 24 h (*t*-test, one-tailed, paired,  $p = 0.011$ ,  $n = 3$ ) and after 48 h (*t*-test, one-tailed, paired,  $p = 0.006$ ,  $n = 3$ ); bars represent mean values  $\pm$  s.e. **b**, Normalized mean integrated fluorescence within the cells is significantly higher after 24 h (*t*-test, one-tailed, paired,  $p = 0.002$ ,  $n = 3$ ) and after 48 h (*t*-test, one-tailed, paired,  $p = 0.012$ ,  $n = 3$ ); bars represent mean values  $\pm$  s.e., the solid line representing WYRGRL-PPS, and the dashed line YRLGRW-PPS nanoparticles. **c**, The ratios of targeted WYRGRL-PPS versus non-targeted YRLGRW-PPS in the ECM (dark grey bars) and within the cells (white bars); bars represent mean values  $\pm$  s.d. There was a 44.8-fold higher targeted nanoparticle accumulation after 24 h and a 71.7-fold mean increase after 48 h. After 96 h, there was a mean 27.6-fold more integrated fluorescence for the green targeted nanoparticles in the ECM than for red non-targeted. **d**, The ratios of extracellular versus intracellular accumulation of targeted and non-targeted nanoparticles; bars represent mean values  $\pm$  s.d. The majority of targeted nanoparticles could be found within the extracellular space (dark grey bars) as indicated by a ratio  $> 1$ . In contrast, most non-targeted nanoparticles detected were located in the cells as indicated by a ratio  $< 1$ .

a barrier to entry, as well as the rapid clearance of molecules out of the joint. To overcome these limitations for intra-tissue bioavailability of therapeutic molecules, drug delivery faces two critical challenges: the size of the delivery system and its retention in the cartilage matrix. Here, we have used biomolecular engineering to create a novel drug-delivery system for intra-tissue drug delivery, here in articular cartilage, which can be made sufficiently small to enter the cartilage matrix and which is further modified with the targeting peptide WYRGRL for binding to the cartilage matrix.

Several methods exist for affinity selection of binding proteins or peptides such as phage display<sup>12</sup>, yeast surface display<sup>23</sup>, messenger RNA display<sup>24</sup> or peptide-on-bead display<sup>25</sup>. Here, phage display using the fUSE5/6-mer library based on the filamentous phage vector fd-tet<sup>21</sup> was used, and the peptide sequence WYRGRL was identified, which was shown to bind specifically to articular cartilage *in vitro* (Fig. 1b). Binding of WYRGRL is sequence specific rather than for example mediated by the net positive charge of the peptide. This is demonstrated in Fig. 2a, which shows that 10  $\mu$ M of WYRGRLC resulted in a decrease of phage titre by almost two orders of magnitude, whereas 10  $\mu$ M of YRLGRWC did not. This is reproduced in the affinity purification experiment, in which

purification of the cartilage matrix with WYRGRLC immobilized in a Sepharose 6B column resulted in a single strong band. In contrast, purification with the scrambled peptide YRLGRWC gave only a faint band at the same size (Fig. 2c). Furthermore, identification of the band by ion-trap mass spectrometry revealed that the sequence WYRGRL binds to collagen II  $\alpha 1$  (see Supplementary Information, Table S1 and Fig. S1). We have thus discovered a short peptide with specific binding to collagen II in articular cartilage.

Targeting the ECM of articular cartilage essentially depends on the ability of the drug-delivery system to enter the cartilage matrix and to stay there. In passive targeting, the distribution of nanoparticles in the joint is mainly governed by the capability of tissue penetration and cellular uptake. Whereas larger particles do not enter, smaller ones are apparently able to penetrate and reside in the cartilage matrix. We demonstrated that nanoparticles with a mean volume diameter of 31 and 38 nm are able to enter the articular cartilage ECM, whereas larger nanoparticles, with a mean volume diameter of 96 nm, could not (Fig. 6). These results are consistent with the literature on viral gene delivery to the cartilage: it has been demonstrated that adeno-associated viruses, with a mean diameter of 20–25 nm, enter the articular cartilage matrix

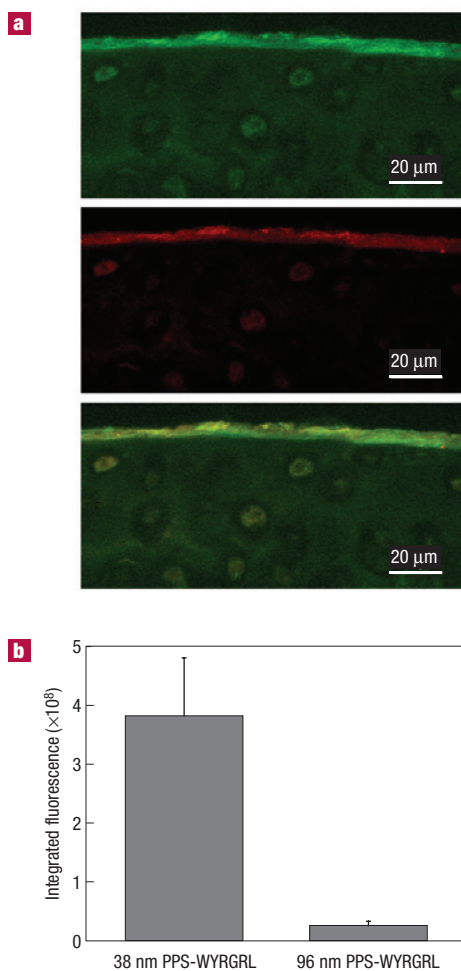


**Figure 6** Size-dependent matrix accumulation of WYRGRL-PPS after 24 h.

**a**, Nanoparticles with a mean size of 96 nm (red channel) were unable to enter the cartilage matrix and were mainly retained at the dense cartilage surface. The green channel represents nanoparticles 38 nm in size. **b**, Quantification of integrated fluorescence revealed a 14.9-fold higher accumulation of 38 nm than 96 nm particles (*t*-test, one-tailed, paired,  $p = 0.037$ ,  $n = 4$ ). Most of the fluorescence measured for 96 nm particles could be attributed to the cartilage surface. The few nanoparticles of the 96 nm batch that had entered the cartilage matrix and had also accumulated in some cells may belong to the lower end of the size distribution and may therefore be substantially smaller than the average size of 96 nm.

up to a depth of penetration of 450  $\mu\text{m}$  in normal and 720  $\mu\text{m}$  in degraded bovine cartilage<sup>26</sup>.

Although both targeted and non-targeted PPS nanoparticles enter the articular cartilage matrix through convective transport due to dynamic compression during ambulation, only the targeted nanoparticles are immobilized within the cartilage matrix, here up to 96 h without statistically significant clearance (Fig. 5c,d). This is shown by the fact that there are up to 71-fold more targeted nanoparticles in the ECM than non-targeted (Fig. 5c). The non-targeted nanoparticles in turn leave the extracellular space and are mainly retained in the intracellular compartment (Fig. 5d). Both targeted and non-targeted nanoparticles are internalized by chondrocytes by a currently unknown mechanism, be it for example receptor-mediated endocytosis via nanoparticle-adsorbed proteins or via macropinocytosis. The literature suggests that this could be influenced by the small size of the nanoparticles<sup>27,28</sup>

or through a scavenger receptor on the cells<sup>29</sup>. Binding of the particles specifically to collagen II is furthermore supported by the observation that the pericellular matrix is deficient in bound nanoparticles: it has been shown that the pericellular matrix surrounding chondrocytes contains almost no collagen II, but mainly consists of collagen VI (ref. 30). Although all *in vitro* experiments have been carried out on bovine cartilage, bovine collagen II is represented with a homology of 92% in murine and 94% in human collagen II, and comparable binding of WYRGRL to murine and human collagen II can therefore be expected.

Intra-articular drug delivery has been termed a major challenge owing to the short residence times of drugs injected within the joint space and therefore rapid uptake of the drugs by the lymphatic circulation, accounting for low bioavailability and potentially adverse systemic effects. Despite the need for the development of formulations for intra-articular controlled release, few reports exist on such use of sustained-release formulations<sup>31–37</sup>, which range from 265 to 490 nm. Given the dense collagen II network with a pore size of about 60 nm in the superficial zone<sup>6</sup>, nanoparticles beyond this size would not be expected to efficiently enter the cartilage matrix, as demonstrated in Fig. 6.

In contrast, the functionalized nanoparticles targeted for the cartilage matrix in this study are sufficiently small to enter the matrix and use it as a reservoir, which offers advantages such as a higher bioavailability of drugs in the cartilage matrix itself. Conjugating a bioaffinity ligand to the nanoparticle surface hinders the nanoparticles from leaving the cartilage matrix. This system therefore provides an intra-tissue release of a therapeutic agent rather than just an intra-articular drug release. Because convective transport of solutes into cartilage is impaired owing to the inherent properties of this tissue<sup>38,39</sup>, the bioavailability of drugs in the cartilage matrix, which is the primary site of the disease process in osteoarthritis, can be enhanced by sustained-release systems that reside in the matrix itself. Besides general intra-articular drug delivery, targeting of the cartilage matrix is therefore especially suited for treatment of early events of cartilage degradation and is likely to be an important factor in future pharmaceutical approaches for the treatment of osteoarthritis.

## METHODS

### MATERIALS

The phage display library fUSE5/6-mer based on filamentous phage strain fd-tet was received from the laboratory of G. P. Smith, Division of Biological Sciences, University of Missouri, Columbia. Cartilage grafts, synovial fluid and synovial membrane were collected from bovine shoulders obtained from the local slaughterhouse. Cartilage grafts were stored in 0.1% sodium azide and protease inhibitors at 4 °C and used within 72 h. Solvents and reagents for nanoparticle synthesis were purchased from Sigma-Aldrich. The peptides WYRGRLC and YRLGRWC (synthesis chemicals from Novabiochem) were synthesized on solid resin using an automated peptide synthesizer (Chemspeed PSW 1100) with standard F-moc chemistry. The amino-terminal amino acids are acetylated and a cysteine residue is added to the C-terminal end of the original sequence for bioconjugation to thiol-reactive functional groups, that is, vinyl sulphone. Purification was carried out on a Waters ultrapurification system using a Waters Atlantis dC<sub>18</sub> semi-preparative column and peptides collected according to their molecular mass analysed by time-of-flight mass spectrometry.

### SCREENING OF PHAGE-DISPLAYED COMBINATORIAL PEPTIDE LIBRARY AND BINDING ASSAYS

Peptides for binding to the articular cartilage matrix were selected by exposing a fUSE5/6-mer library to bovine cartilage grafts, which provided  $6.4 \times 10^7$  different phage clones with 6-amino acid linear-peptide inserts displayed on the minor coat protein of a filamentous phage<sup>12,21</sup>. Cartilage grafts were collected with 8 and 4 mm biopsy cutters (two-sided surface 1 cm<sup>2</sup> and 0.25 cm<sup>2</sup>). A total of five screening rounds was carried out. In the first round,  $10^{13}$  and in subsequent rounds  $10^{12}$  phage virions per millilitre were exposed to the cartilage graft, washed with PBS/Tween 20 and eluted at low pH (buffers used and details

in the Supplementary Information). Between panning rounds, stringency was increased (see the Supplementary Information). Eluted phage was amplified overnight in *Escherichia coli* strain TG1 in 2xYT medium and purified by two times polyethylene glycol/NaCl (2M, 25%) precipitation. Quantitative titre counts were obtained by spot titring of 15 µl of phage/bacterial culture onto LB agar/tetracyclin plates and are given in transducing units per millilitre. Binding assays were carried out as explained in the Supplementary Information.

#### AFFINITY PURIFICATION AND PROTEIN IDENTIFICATION

Bovine cartilage was incubated with collagenase D at 1 mg ml<sup>-1</sup> overnight at 37 °C with mild agitation. 167 mg of thiopropyl Sepharose 6B (GE Healthcare Bio-Sciences) was prepared according to the manufacturer's instructions to give a 0.5 ml gel. 15 mg of peptide, either WYRGRLC or YRLGRWC, was immobilized in the gel. After washing, the soluble fraction of cartilage ECM proteins was added and incubated in the gel for 1 h. Elution was carried out after thorough washing with PBS with 10, 50, 125 and 500 mM KCl and the fractions collected. The fractions were analysed by SDS-PAGE with a 7.5% gel and stained with Coomassie. For mass spectrometry, the band was cut out and in-gel digested (see the Supplementary Information). Samples were then analysed using an Advion BioSystems electrospray ion source coupled to a Thermo Fisher Scientific LTQ linear ion-trap mass spectrometer. The tryptic digests were infused in electrospray ionization mass spectrometry (ESI + MS) and ESI + MS\MS mode using helium as the collision gas. The collected data were analysed for protein identification using the Bioworks software package from Thermo Fisher Scientific.

#### SYNTHESIS OF NANOPARTICLES

Poly(propylene sulphide) nanoparticles were prepared as described elsewhere<sup>18</sup>. Surface functionalization is explained in detail in the Supplementary Information.

#### CONFOCAL MICROSCOPY AND IMAGE ANALYSIS

*In vivo* injection into murine knee joints and sample preparation is explained in the Supplementary Information. The sections were analysed by confocal laser scanning microscopy using a Zeiss LSM510 META microscope. Gain and offset and laser power were adjusted for the red and green channels with a ×100 diluted 0.5% w/v nanoparticle stock solution containing green-labelled WYRGRL-PPS and red-labelled YRLGRW-PPS to adjust for differences in fluorescence emission. The integrated fluorescence for a sample containing the same amount of green-labelled and red-labelled nanoparticles was therefore equal, which is required for quantification (see Supplementary Information, Fig. S3a). All imaging was carried out using these settings in a temperature-controlled environment. Images for analysis were obtained using a Zeiss ×63 Aplanachromat objective in 10 different locations per joint with a z stack of 10 images each (voxel size  $x$ - $y$  0.29 µm,  $z$  0.7 µm). Background fluorescence was determined by imaging a cryosection slide of a joint not injected with nanoparticles. Background was subsequently subtracted for each channel and in each section before quantification of fluorescence (see Supplementary Information Fig. S3b). Quantification of integrated fluorescence per region of interest on all 10 planes was carried out using Metamorph (Molecular Devices) (details in the Supplementary Information). For further analysis, the integrated fluorescence per region of interest was normalized to the area (amount of voxels) of each region of interest. Statistical analysis and testing was carried out on SPSS 11 for Macintosh.

Received 17 July 2007; accepted 7 January 2008; published 3 February 2008.

#### References

- Bae, Y. *et al.* Preparation and biological characterization of polymeric micelle drug carriers with intracellular pH-triggered drug release property: Tumor permeability, controlled subcellular drug distribution, and enhanced *in vivo* antitumor efficacy. *Bioconjug. Chem.* **16**, 122–130 (2005).
- Dreher, M. R. *et al.* Tumor vascular permeability, accumulation, and penetration of macromolecular drug carriers. *J. Natl Cancer Inst.* **98**, 335–344 (2006).
- Duncan, R. The dawning era of polymer therapeutics. *Nature Rev. Drug. Discov.* **2**, 347–360 (2003).
- Shiah, J. J., Sun, Y., Peterson, C. M. & Kopecek, J. Biodistribution of free and N-(2-hydroxypropyl)methacrylamide copolymer-bound mesochlorin e(6) and adriamycin in nude mice bearing human ovarian carcinoma OVCAR-3 xenografts. *J. Control Release* **61**, 145–157 (1999).
- Owen, S. G., Francis, H. W. & Roberts, M. S. Disappearance kinetics of solutes from synovial fluid after intra-articular injection. *Br. J. Clin. Pharmacol.* **38**, 349–355 (1994).
- Comper, W. D. in *Cartilage: Molecular Aspects* (eds Hall, B. & Newman, S.) 59–96 (CRC Press, Boston, 1991).
- Torzilli, P. A., Arduino, J. M., Gregory, J. D. & Bansal, M. Effect of proteoglycan removal on solute mobility in articular cartilage. *J. Biomech.* **30**, 895–902 (1997).

- Arap, W. *et al.* Steps toward mapping the human vasculature by phage display. *Nature Med.* **8**, 121–127 (2002).
- Kay, B. K., Kasanov, J. & Yamabhai, M. Screening phage-displayed combinatorial peptide libraries. *Methods* **24**, 240–246 (2001).
- Kolonin, M. G. *et al.* Synchronous selection of homing peptides for multiple tissues by *in vivo* phage display. *FASEB J.* **20**, 979–981 (2006).
- Pasqualini, R. & Ruoslahti, E. Organ targeting *in vivo* using phage display peptide libraries. *Nature* **380**, 364–366 (1996).
- Smith, G. P. & Petrenko, V. A. Phage display. *Chem. Rev.* **97**, 391–410 (1997).
- Cherney, R. J. *et al.* Potent and selective aggrecanase inhibitors containing cyclic P1 substituents. *Bioorg. Med. Chem. Lett.* **13**, 1297–1300 (2003).
- Noe, M. C. *et al.* Discovery of 3,3-dimethyl-5-hydroxypiperidic hydroxamate-based inhibitors of aggrecanase and MMP-13. *Bioorg. Med. Chem. Lett.* **15**, 2808–2811 (2005).
- Noe, M. C. *et al.* Discovery of 3-OH-3-methylpiperidic hydroxamates: Potent orally active inhibitors of aggrecanase and MMP-13. *Bioorg. Med. Chem. Lett.* **15**, 3385–3388 (2005).
- Noe, M. C. *et al.* 3-Hydroxy-4-arylsulfonyltetrahydropyran-3-hydroxamic acids are novel inhibitors of MMP-13 and aggrecanase. *Bioorg. Med. Chem. Lett.* **14**, 4727–4730 (2004).
- Yao, W. *et al.* Design and synthesis of a series of (2R)-N(4)-hydroxy-2-(3-hydroxybenzyl)-N(1)-[(1S,2R)-2-hydroxy-2,3-dihydro-1H-inden-1-yl]butanediamide derivatives as potent, selective, and orally bioavailable aggrecanase inhibitors. *J. Med. Chem.* **44**, 3347–3350 (2001).
- Rehor, A., Hubbell, J. A. & Tirelli, N. Oxidation-sensitive polymeric nanoparticles. *Langmuir* **21**, 411–417 (2005).
- Rehor, A. *Poly(propylene sulfide) Nanoparticles as Drug Carriers*. Thesis, Swiss Federal Institute of Technology (2005).
- Wieland, H. A., Michaelis, M., Kirschbaum, B. J. & Rudolph, K. A. Osteoarthritis—an untreatable disease? *Nature Rev. Drug. Discov.* **4**, 331–344 (2005).
- Zacher, A. N. 3rd, Stock, C. A., Golden, J. W. 2nd & Smith, G. P. A new filamentous phage cloning vector: fd-tet. *Gene* **9**, 127–140 (1980).
- Lutolf, M. P. & Hubbell, J. A. Synthesis and physicochemical characterization of end-linked poly(ethylene glycol)-co-peptide hydrogels formed by Michael-type addition. *Biomacromolecules* **4**, 713–722 (2003).
- Boder, E. T. & Witttrup, K. D. Yeast surface display for screening combinatorial polypeptide libraries. *Nature Biotechnol.* **15**, 553–557 (1997).
- Xu, L. *et al.* Directed evolution of high-affinity antibody mimics using mRNA display. *Chem. Biol.* **9**, 933–942 (2002).
- Lam, K. S., Lebl, M. & Krchnak, V. The “one-bead-one-compound” combinatorial library method. *Chem. Rev.* **97**, 411–448 (1997).
- Madry, H., Cucchiari, M., Terwilliger, E. F. & Trippel, S. B. Recombinant adeno-associated virus vectors efficiently and persistently transduce chondrocytes in normal and osteoarthritic human articular cartilage. *Hum. Gene Ther.* **14**, 393–402 (2003).
- Gao, H., Shi, W. & Freund, L. B. Mechanics of receptor-mediated endocytosis. *Proc. Natl Acad. Sci. USA* **102**, 9469–9474 (2005).
- Lynch, I., Dawson, K. A. & Linse, S. Detecting cryptic epitopes created by nanoparticles. *Sci. STKE* **2006**, pe14 (2006).
- Nagayama, S. *et al.* Fetuin mediates hepatic uptake of negatively charged nanoparticles via scavenger receptor. *Int. J. Pharm.* **329**, 192–198 (2007).
- Guilak, F. *et al.* The pericellular matrix as a transducer of biomechanical and biochemical signals in articular cartilage. *Ann. NY Acad. Sci.* **1068**, 498–512 (2006).
- Phillips, N. C., Thomas, D. P., Knight, C. G. & Dingle, J. T. Liposome-incorporated corticosteroids. II. Therapeutic activity in experimental arthritis. *Ann. Rheum. Dis.* **38**, 553–557 (1979).
- Shaw, I. H., Knight, C. G., Thomas, D. P., Phillips, N. C. & Dingle, J. T. Liposome-incorporated corticosteroids. I. The interaction of liposomal cortisol palmitate with inflammatory synovial membrane. *Br. J. Exp. Pathol.* **60**, 142–150 (1979).
- Ratcliffe, J. H., Hunneyball, I. M., Smith, A., Wilson, C. G. & Davis, S. S. Preparation and evaluation of biodegradable polymeric systems for the intra-articular delivery of drugs. *J. Pharm. Pharmacol.* **36**, 431–436 (1984).
- Ratcliffe, J. H., Hunneyball, I. M., Wilson, C. G., Smith, A. & Davis, S. S. Albumin microspheres for intra-articular drug delivery: Investigation of their retention in normal and arthritic knee joints of rabbits. *J. Pharm. Pharmacol.* **39**, 290–295 (1987).
- Tuncay, M. *et al.* *In vitro* and *in vivo* evaluation of diclofenac sodium loaded albumin microspheres. *J. Microencapsul.* **17**, 145–155 (2000).
- Horisawa, E. *et al.* Prolonged anti-inflammatory action of DL-lactide/glycolide copolymer microspheres containing betamethasone sodium phosphate for an intra-articular delivery system in antigen-induced arthritic rabbit. *Pharm. Res.* **19**, 403–410 (2002).
- Horisawa, E. *et al.* Size-dependency of DL-lactide/glycolide copolymer particulates for intra-articular delivery system on phagocytosis in rat synovium. *Pharm. Res.* **19**, 132–139 (2002).
- Quinn, T. M., Morel, V. & Meister, J. J. Static compression of articular cartilage can reduce solute diffusivity and partitioning: Implications for the chondrocyte biological response. *J. Biomech.* **34**, 1463–1469 (2001).
- Quinn, T. M., Kocian, P. & Meister, J. J. Static compression is associated with decreased diffusivity of dextrans in cartilage explants. *Arch. Biochem. Biophys.* **384**, 327–334 (2000).

#### Acknowledgements

The authors thank V. Garea and M. Pasquier for the help with the animal work and histology, A. Rehor for help with and discussions on initial nanoparticle synthesis, R. Schoenmakers for peptide synthesis, A. van der Vlies for obtaining <sup>1</sup>H-NMR spectra, and especially the BIOP core facility for their support in establishing the imaging and quantification protocol and the proteomics core facility for running mass spectrometry analyses, and M. Lutolf for his help and suggestions in preparing the manuscript. DAR was supported by a grant from the Hans-Neuenschwander-Stiftung, Berne. Correspondence and requests for materials should be addressed to J.A.H. Supplementary Information accompanies this paper on [www.nature.com/naturematerials](http://www.nature.com/naturematerials).

#### Author contributions

The experiments have been designed by D.A.R. and J.A.H. and carried out by D.A.R. H.B. introduced phage display and aided in establishing initial protocols. C.P.O. assisted in the affinity purification. The manuscript was written by D.A.R. and J.A.H. Principal investigator is J.A.H.

#### Competing financial interests

The authors declare competing financial interests: details accompany the full-text HTML version of the paper at [www.nature.com/naturematerials/](http://www.nature.com/naturematerials/).

Reprints and permission information is available online at <http://ngp.nature.com/reprintsandpermissions/>